Journal of Low Temperature Physics, Vol. 124, Nos. 1/2, 2001

Analysis of the Melting Process of Magnetized Solid ^{3}He

E.R. Plomp, R. van Rooijen, H. Akimoto[§], G. Frossati, R. Jochemsen and W. van Saarloos*

Kamerlingh Onnes Laboratory, Leiden University, P.O. Box 9504,
**Lorentz Institute, Leiden University, P.O Box 9506,*
2300 RA Leiden, The Netherlands

We report on our analysis of the melting process of highly magnetized solid ^{3}He. Akimoto et al. found that the solid-liquid interface becomes unstable during melting in a magnetic field of 9 T. The liquid then penetrates into the solid in the form of cellular dendrites. The instability, which was predicted by Puech et al., was attributed to a Mullins-Sekerka type of instability due to the magnetization gradient on the solid side. The measurements on which we base our analysis clearly show gradients on both sides of the interface. We present an extension of the linear stability analysis for this situation, as well as a numerical calculation of the dispersion relation of interface deformations. Our results are in good agreement with the experiment and explain the initial suppression of the instability, caused by the magnetization gradient in the liquid.

PACS numbers: 67.80.Jd, 67.65.+z, 68.45 -v, 47.54.+r, 47.20.Ma.

1. INTRODUCTION

Because the effective Fermi temperature of liquid ^{3}He is large compared to the nuclear magnetic moment ($T_F/\mu_3 > 175$ Tesla), it is impossible to obtain significantly magnetized liquid ^{3}He by the *brute force* method ("cool as low as possible at the maximum available magnetic field"). The best method to produce highly magnetized liquid ^{3}He is the melting of solid ^{3}He in a high magnetic field.[1] Since the solid behaves almost as a Curie paramagnet down to a few milliKelvin, a magnetization of 80% can be obtained at T = 5 mK in a field of 9 T. Therefore Castaing and Nozières[2] suggested the rapid melting method to study the magnetization dependence of the

strongly correlated ^{3}He Fermi liquid. Although the high magnetization of the liquid is produced in a non-equilibrium situation, the relaxation of the magnetization is a relatively slow process ($T_{1,l} \approx 50 - 1000$ s). This spin lattice relaxation time is much longer than any microscopic relaxation time in the system, which allows thermodynamic and transport measurements, while the magnetization slowly decays.[1,3]

Of course the melting of the solid must take place on a time scale shorter than $T_{1,l}$. In their seminal paper, Castaing and Nozières[2] suggest a melting scenario in which an enhanced magnetization boundary layer is built up on the solid side of the interface. This boundary layer is caused by the increased magnetization of the just produced liquid. The equality of chemical potentials of liquid and solid at the interface is guaranteed by the sufficiently rapid exchange of spins at the interface on a microscopic scale, and thus the solid obtains a boundary layer with enhanced magnetization during melting. The width of this layer is given by the magnetization diffusion length $\ell_s = D_s/V$, where V is the velocity of the melting interface, and D_s the diffusion coefficient in the solid. Since the magnetization influences the melting pressure, this situation is very similar to the generic case of a gradient driven growth problem.[4,5] Bonfait *et al.*[6] suggested that in analogy to the usual case of solidification, the build-up of this boundary layer would render the interface unstable. This suggestion was backed up by a calculation of Puech *et al.*.[7] The situation they analyzed, sketched in Fig. 1(a), is the one often used in theoretical considerations,[4,5] namely that of a planar interface propagating with constant speed in the absence of gradients behind the interface. The Mullins-Sekerka type analysis of Puech *et al.*[7] for this case predicted that the interface would be unstable with a typical growth time for the most unstable modes of the order of 0.1 seconds.

It was shown by Marchenkov *et al.*[8] that this predicted instability of the interface of melting magnetized solid ^{3}He indeed exists. Since the instability was not seen in zero magnetic field during melting of solid with the same initial temperature, it was concluded that the magnetization and thus the induced gradient is indeed the cause of the instability. A question that remained was the late occurrence of the interface instability, often after a significant fraction of the solid had melted.

This question was addressed by Akimoto *et al.*[9] by performing a rapid melting experiment in a strong magnetic field with a small magnetic field gradient. Growing the solid with a horizontal interface, they were able to obtain information about the magnetization profile along the direction normal to the interface. Qualitatively the results are sketched in Fig. 1(b), in which the most notable agreement with Fig. 1(a) is the enhanced magnetization in the boundary layer in the solid. These measurements therefore provide a

direct experimental confirmation of the scenario suggested by Castaing and Nozières.[2] Two main differences are the relaxation of the solid magnetization during the melting, and the strong magnetization gradient in the liquid, caused by the fact that the melting doesn't start from an all-solid situation. Akimoto *et al.*[9] convincingly but qualitatively argued that the delay in the instability was caused by the strong gradient in the liquid magnetization. In this paper we present a quantitative analysis of the melting scenario.

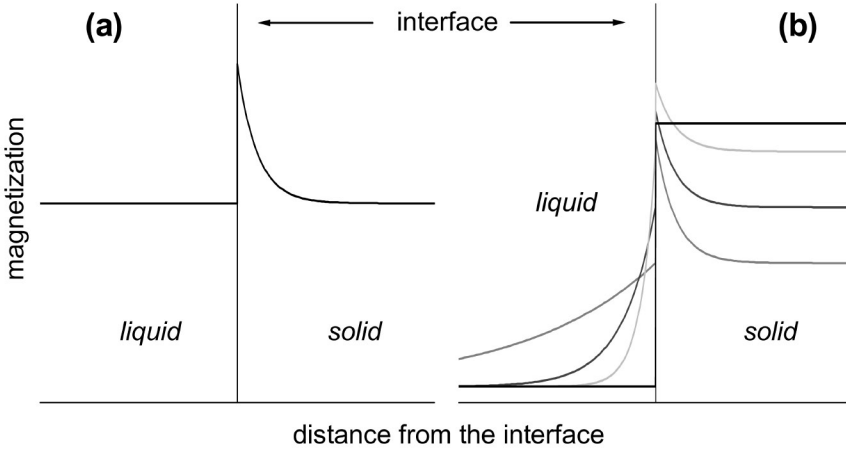

Fig. 1. (a) Sketch of the magnetization profile of a planar interface melting with a constant speed, for which Puech *et al.*[7] performed a linear stability analysis. The magnetization profile falls off exponentially in the solid, while there is no gradient in the liquid. (b) Sketch of the build-up of the magnetization profiles as concluded from the experiments of Akimoto *et al.*,[9] at the moment the melting starts (black line) and at three successive times during the initial melting phase. Note that while the boundary layer in the solid is building up, a *stabilizing* gradient is also building up in the liquid. In the bulk of the solid the magnetization relaxes due to the increase in the temperature. Both pictures are drawn in a frame moving with the interface.

In the next section we recall the experimental conditions.[9] In Section 3 we extend the linear stability analysis and derive the wave number dependence of the temporal growth coefficient. Also, we discuss how far the physics can be understood from the approximation that the characteristic length of the instability is in between the diffusion lengths of the two phases and compare the numerical calculations with the experimental results. A discussion of some aspects of this analysis forms the concluding section.

2. EXPERIMENT

The cryostat used in the experiments has been developed for optical observations in strong magnetic fields at ultralow temperatures. It contains a nuclear demagnetization stage, a 9 T magnet and an optical system. The lowest temperature reached is 65 μK in zero magnetic field. The ^{3}He could not be cooled below 0.6 mK due to a heat leak of 200 pW caused by the camera. In maximum field the liquid ^{3}He can be cooled to 2 mK while taking images every 5 s. The optical part consists of a LED, thermally anchored at the 1 K pot, optical fibers, a beam expander attached to the 50 mK shield, "cold" mirrors just outside the cell and a CCD camera located inside the IVC at 65 K. The setup is described elsewhere[10] in much more detail.

The sample cell is a Frossati-style compressional cell. It is thermally anchored to the nuclear stage and contains a silver/platinum sinter. The volume of the ^{3}He space can be varied by changing the pressure on the ^{4}He side of a flexible cylindrical Kapton membrane with a thickness of about 130 μm. On the melting curve this results in ^{3}He crystal growth or melting. The pressure is measured by a sapphire pressure gauge located at the top of the cell. Also, a vibrating wire viscometer has been installed in the upper part. The optical part of the cell is situated below the Pomeranchuk part. It consists of a white Araldite body containing two Suprasil windows, 3 mm apart. The temperature was measured with a carbon resistance thermometer at the bottom of the optical cell. Fig. 2 shows a schematic view.

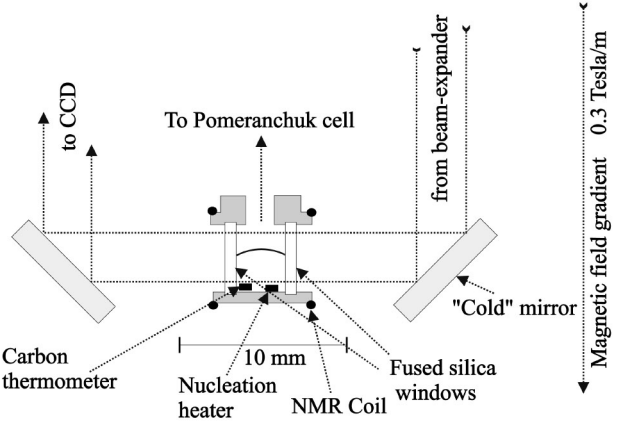

Fig. 2. Schematic drawing of the optical part of the cell. The dotted lines indicate the light beam. In between the windows the solid-liquid interface has been drawn. The curvature is somewhat exaggerated.

The solid was grown by slowly compressing the ^{3}He chamber. To start solidification at the bottom of the cell and to keep the interface horizontal during growth, a heat input of about 20 nW was provided by the nucleation heater. After growing, the solid was left to relax for about 6 hours to get the interface as flat as possible. Sometimes a small amount of solid was melted to obtain a smooth interface. As indicated in Fig. 2, it is not completely horizontal but rounded due to adhesion. The difference in height between the top of the interface and the place where it touches the windows is only about 0.3 mm.

Fig. 3 shows the time-trace for this decompression. The pressure was reduced from 34 bar to 30 bar in 60 s. The initial temperature was 8 mK. Because of a problem with the lower thermometer, the temperatures have been taken from another decompression, with a similar depressurization rate. We measured the total magnetization in the cell. Because of the difference in relaxation times between the solid and the liquid phase, the magnetization decay changes slope around the instability. This happens around 50 s, when there is still a significant amount of solid ^{3}He in the cell.

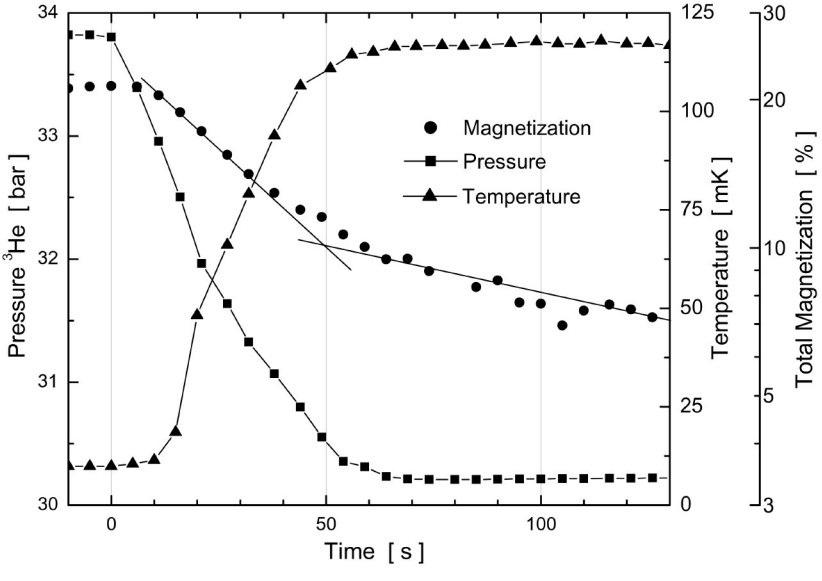

Fig. 3. The time evolution of the pressure and the total magnetization in the optical cell during the decompression shown in Fig. 4. The temperature trace is obtained from a decompression with a similar pressure evolution, fraction of solid and starting temperature.

Fig. 4 shows a series of images taken during a rapid decompression. Pictures are taken every 5 s with an aperture time of 1.2 s. The image size is 240 × 240 pixels. The diameter of the light beam is 3 mm, so the resolution is about 13 μm. The thick black line on the images is due to reflections. The bottom of this line is identified with the liquid-solid interface. The first frame is taken at equilibrium before melting. For about 40 s the interface remains smooth and horizontal. Although some structure in the solid can be seen before, the system is not fully unstable until 45 s after the beginning of the decompression. At that time cellular dendrites appear from the interface in the vertical direction. The typical size is 50 - 100 μm.

A gradient coil has been installed to measure magnetization profiles. A field gradient of 0.3 T/m is applied vertically, parallel to the 9 T field. The pickup coil around the optical part of the cell (see Fig. 2) is tuned at 287 MHz. The magnetization is then measured by the NMR absorption during a frequency sweep. This provides cross-sections through slices perpendicular to the vertical z-direction, parallel to the interface. Profiles are measured at regular intervals. Some are depicted in Fig. 5, in which the right-hand side corresponds with the bottom part of the cell. At equilibrium the magnetization of the solid is much higher than that of the liquid. It drops over a region of 0.3 mm, indicating that the interface was slightly curved and tilted. During melting the interfacial region shifts to the right and a boundary layer builds up in the solid. Also, the bulk solid magnetization relaxes and the gradient in the liquid decreases. At the time at which the instability occurs, the gradient in the liquid has decreased substantially and the bulk solid magnetization is about the same as that of the liquid near the interface.

3. THEORY

3.1. Mullins-Sekerka Instability

The Mullins-Sekerka linear stability analysis[11] was originally developed to investigate the stability of a moving planar interface during the freezing of an alloy. In a diffusion driven system the progression of an arbitrary perturbation of the interface is calculated. The general idea is that a gradient in front of a moving interface will lead to an instability. A small outward ripple will compress the isotherms and therefore increase the gradient. This will increase the heat flow and thus favor growth at that particular spot. As a result dendrites will be formed.

For ^{3}He below the minimum of the melting curve the latent heat is negative and therefore both the direction of the heat flow and the sign of

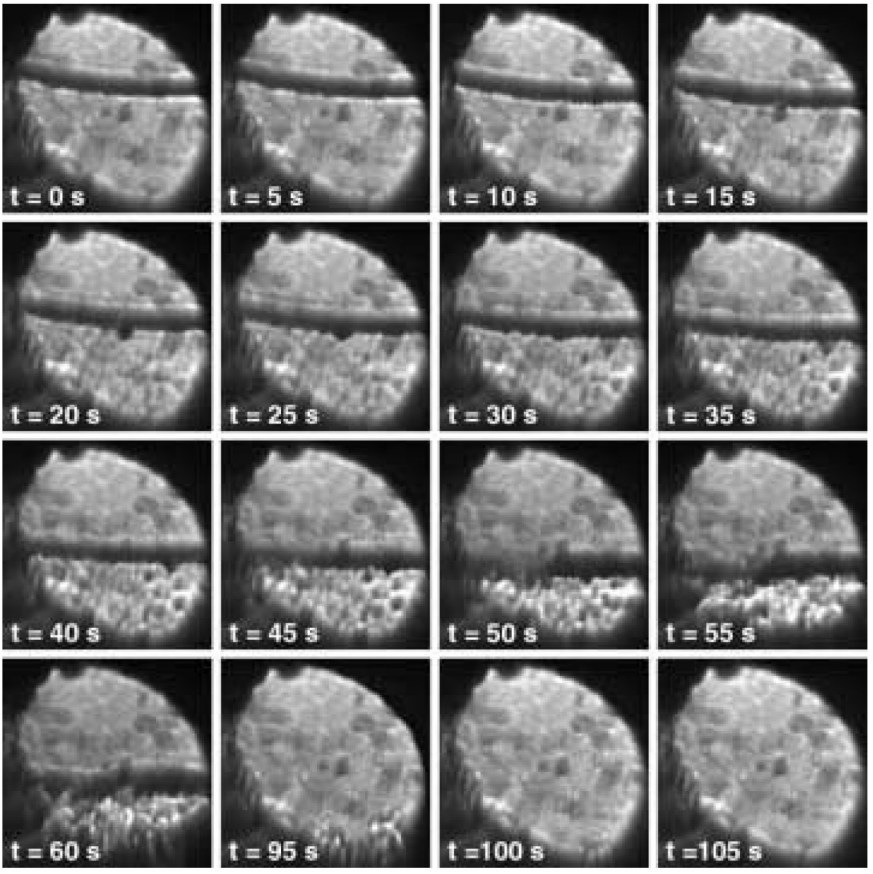

Fig. 4. Optical images during a rapid melting experiment of solid ^{3}He in a 8.9 T magnetic field, taken with an aperture time of 1.2 s. The bottom of the thick black line marks the interface of the solid in the lower part of the cell. The sample cell has a width of 3 mm between the optical windows. The instability occurs around 45 s after the start of the decompression. All solid has disappeared after 100 s (last three images).

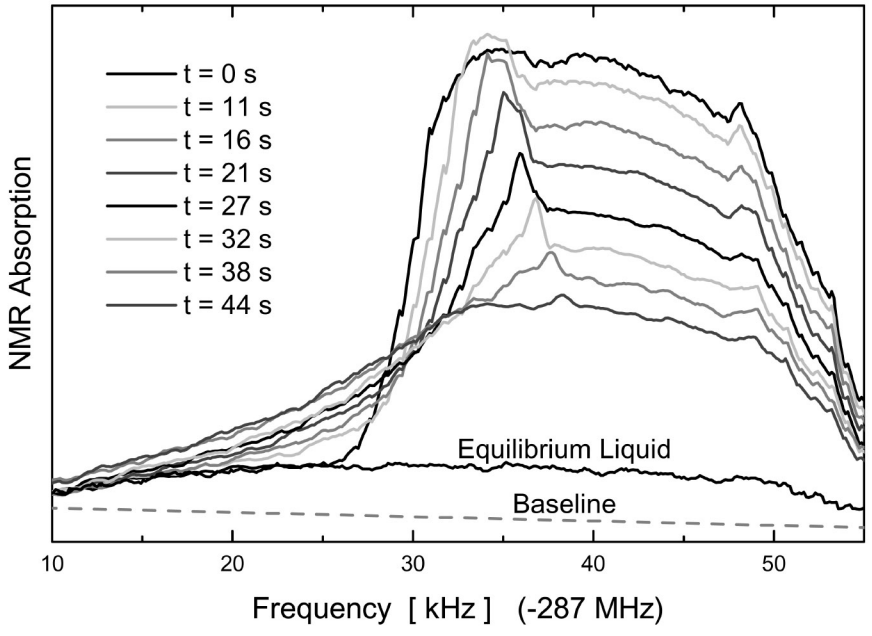

Fig. 5. A selection out of the magnetization profiles measured during the same rapid melting experiment as shown in Figs. 3 and 4. The vertical field gradient is 0.3 T/m, which corresponds to 10 kHz/mm. The initial temperature is 8 mK and the magnetic field is 8.9 T.

the temperature gradient are reversed. Solidification will therefore still be dendritic,[12] whereas melting will generally be smooth. If however the liquid is magnetized and then rapidly melted, an instability will occur.[7] To describe this, the Mullins-Sekerka model will be used. The driving force will now be the (relative) magnetization field. The derivation of the dispersion relation below largely follows that of Puech *et al.*,[7] except for the shape of the magnetization profile, in which the magnetization gradient in the liquid is now included.

We consider a planar interface moving in the solid direction z. We assume pure diffusive transport (no convection) in the bulk phases. The magnetization diffusion coefficients D_i in phase i ($i = s, l$) are defined through:

$$D_i \frac{\partial^2 m_i}{\partial z^2} = \frac{\partial m_i}{\partial t} \tag{1}$$

with m_i the magnetization field (relative to the maximum magnetization). In the frame moving with the interface in the positive z-direction ($z \to z - Vt$)

the diffusion equations are:

$$D_i \frac{\partial^2 m_i}{\partial z^2} + V \frac{\partial m_i}{\partial z} = \frac{\partial m_i}{\partial t} \tag{2}$$

with the (constant) planar interface velocity V. Conservation of magnetization across the interface is expressed by:

$$V(m_s(0) - m_l(0)) = -D_s \frac{\partial m_s}{\partial z}(0) + D_l \frac{\partial m_l}{\partial z}(0) \tag{3}$$

The left-hand side represents the magnetization density flux across the interface in the direction of increasing z due to the displacement of the interface, the right-hand side that due to diffusion. If the exchange of particles from one phase to the other is faster than the magnetization relaxation time T_1 the effective fields are equal at the interface. The steady state solutions have to satisfy the diffusion equations (2) (with $\partial m_i/\partial t = 0$), together with these interfacial boundary conditions and the boundary conditions at infinity. We assume these planar solutions (denoted by m^{pl}) to exist for both the solid at $z > 0$ and the liquid at $z < 0$ and to remain unaffected by changes in the interface shape.

We proceed by introducing a harmonic perturbation ξ of infinitesimal amplitude ξ_0 on the interface. For simplicity we take only one direction x in the plane of the interface into account.

$$z = \xi(x,t) = \xi_0 e^{\gamma t + ikx} \tag{4}$$

Instability occurs if any Fourier component of an arbitrary perturbation grows, stability if all decay. The evolution of the mode is determined by the sign of the parameter γ. Associated with this deformation are perturbations δm_i of the magnetization field on both sides, which have to disappear several wavelengths away from the interface. The spatial decay lengths q_i^{-1} are defined through:

$$\delta m_s(z) = \delta_s e^{\gamma t + ikx} e^{-q_s z} \tag{5}$$

$$\delta m_l(z) = \delta_l e^{\gamma t + ikx} e^{q_l z} \tag{6}$$

These are substituted in the diffusion equations (2), giving:

$$\gamma = D_s(q_s^2 - k^2) - V q_s \tag{7}$$

$$\gamma = D_l(q_l^2 - k^2) + V q_l \tag{8}$$

in which q_s and q_l are the positive solutions.

The next step is a linear expansion of the magnetization fields and gradients to first order in ξ around the planar solutions m_i^{pl} at $z = 0$, which is now the *average* interface position.

$$m_i(\xi) - m_i^{pl}(0) = \delta m_i(0) + \frac{\partial m_i^{pl}}{\partial z}(0)\xi \tag{9}$$

The first term on the right-hand side is the change in magnetization field δ_i at the original position. The second one expresses the fact that as the interface deforms, it explores the steady state field and feels its gradient. This equation reads the same for both phases, indicating that we have included the gradients behind and in front of the interface. The expansions of the gradients are then obtained by derivation with respect to z and using equations (5) and (6):

$$\frac{\partial m_s}{\partial z}(\xi) - \frac{\partial m_s^{pl}}{\partial z}(0) = -q_s \delta m_s - \frac{\partial m_s^{pl}}{\partial z}(0)\frac{V}{D_s}\xi \tag{10}$$

$$\frac{\partial m_l}{\partial z}(\xi) - \frac{\partial m_l^{pl}}{\partial z}(0) = q_l \delta m_l \tag{11}$$

On the solid side the magnetization falls off exponentially, with decay length D_s/V. We neglected the second derivative of m_l^{pl}, assuming that the profile is roughly linear near the interface on the liquid side.

Local equilibrium implies that all thermodynamic relations are valid locally. The changes in magnetization fields on the interface, given by the right-hand side of equation (9) then satisfy the boundary condition (3) with the *instantaneous* interface velocity $v \equiv V + \partial\xi/\partial t$. Also they correspond to equal changes in effective field h:

$$\delta m_i + \frac{\partial m_i^{pl}}{\partial z}(\xi) = \chi_i h \tag{12}$$

in which χ_i is the magnetic susceptibility in phase i, defined as $\partial m_i/\partial H$. Finally, the changes in chemical potential per unit volume μ_i are (α is the surface stiffness):

$$\delta\mu_s = -\alpha k^2 \xi - \phi^{-1} m_s^{pl}(0) h \tag{13}$$

$$\delta\mu_l = -\phi^{-1} m_l^{pl}(0) h \tag{14}$$

Because we use the reduced magnetization the magnetic field is expressed in J/mol. To express it in Kelvins we divide by the perfect gas constant. The scaling factor ϕ then becomes V_m/R. The changes in chemical potential are equal at the interface where there is a free exchange of particles. Therefore we can write:

$$h = -\frac{\alpha\phi k^2}{\Delta m}\xi \tag{15}$$

with $\Delta m \equiv m_s^{pl}(0) - m_l^{pl}(0)$. We can now derive an expression for the temporal growth factor γ, which comes into equation (3) through $v = V + \gamma\xi$. After substitution of all the expansion parameters ξ, δ_s, δ_l, v and h we get:

$$\begin{aligned}\gamma &= -\frac{(D_s q_s - V)}{\Delta m}\frac{\partial m_s^{pl}}{\partial z}(0) - \frac{D_l q_l}{\Delta m}\frac{\partial m_l^{pl}}{\partial z}(0) \\ &- \frac{\alpha\phi k^2}{(\Delta m)^2}(D_s q_s \chi_s + D_l q_l \chi_l + V(\chi_l - \chi_s))\end{aligned} \tag{16}$$

Note that for the same magnetization gradient in the solid as Puech *et al.*[7] ($\frac{\partial m_s^{pl}}{\partial z}(0) = -\Delta m \frac{V}{D_s}$) and no gradient in the liquid ($\frac{\partial m_l^{pl}}{\partial z}(0) = 0$) we reproduce their result. If however the gradient is non-zero (it is always positive from our choice of coordinates), it *reduces* the growth rate γ. As we see in Fig. 1 and Fig. 5, this stabilizing effect is especially significant during the initial transient.

3.2. Quasi-Stationary Approximation

The general result (16) together with the equations for the spatial decay of the magnetization (7) and (8) form the dispersion relation $\gamma(k)$. To evaluate this set we eliminate the parameters q_i using approximations for the length-scale and the time-scale. The magnetization diffusion length ℓ_i in phase i is the decay length in the stationary solutions, defined as:

$$\ell_i \equiv \frac{D_i}{V} \tag{17}$$

We expect the wavelength $\lambda = 2\pi/k$ of the most unstable modes to be in the same order of magnitude as the diameter of the dendrites, for which we have the experimental value of 100 μm.

We assume the wavelength of perturbations that cause the instability to be in the intermediate region (in between the diffusion lengths). This approximation is quite natural in case of temperature fields, but there is no *evident* physical necessity in our case and it will have to be checked afterwards. Since $D_s \ll D_l$:

$$\frac{1}{\ell_l} < k < \frac{1}{\ell_s} \tag{18}$$

We rewrite equations (7) and (8) as:

$$q_s = \frac{1}{2\ell_s} \pm \frac{1}{2\ell_s}\sqrt{1 + 4\ell_s^2(k^2 + \frac{\gamma}{D_s})} \tag{19}$$

$$q_l = -\frac{1}{2\ell_l} \pm k\sqrt{1 + \frac{\gamma}{D_l k^2} + \frac{1}{4\ell_l^2 k^2}} \tag{20}$$

Both q_s and q_l have to be positive, so only the positive roots remain. As noted before, the model is only valid for slowly growing perturbations; only those are accompanied by steady state fields. The relaxation times of the diffusion fields $(D_i k^2)^{-1}$ are then much smaller than the characteristic growth time of the perturbations γ^{-1}. Therefore, close to the instability threshold:

$$\gamma \ll D_s k^2 \tag{21}$$

The expansions of equations (19) and (20) now become:

$$q_s \approx \frac{1}{\ell_s} + \ell_s(k^2 + \frac{\gamma}{D_s}) - \ell_s^3(k^2 + \frac{\gamma}{D_s})^2 \tag{22}$$

$$q_l \approx k - \frac{1}{2\ell_l} + \frac{\gamma}{2D_l k} \tag{23}$$

where we keep the expansion of q_s to first order in γ. After substitution in equation (16) two terms containing χ_s cancel and we get the dispersion relation in explicit form:

$$\gamma\left[1 + \frac{\alpha\phi V^2\chi_l}{4D_s^2(\Delta m)^2 k}\left(1 + \frac{2\chi_s D_s k}{\chi_l V}\right)\right] = \frac{V^2}{2D_s} - \frac{D_l V^2}{2D_s^2(\Delta m)k^2} \times \left(k - \frac{V}{2D_l}\right)\frac{\partial m_l}{\partial z}(0) - \frac{\alpha\phi V^2}{2D_s^2(\Delta m)^2}\left(D_l\chi_l k + \frac{V}{2}\chi_l\right) \tag{24}$$

where we have neglected one term, using that the ratio $D_l\chi_l/D_s\chi_s$ is much larger than 1.

Because of the large thermal conductivity of the solid[13] the temperature measured at the bottom of the cell is equal to that of the interface. Furthermore, we assume the pressure to be uniform throughout the cell. We consider the magnetization profiles to be "frozen in" on the time-scale at which the perturbations grow. This is justified by the experimental observation that the instability occurs suddenly. It allows us to perform calculations on each profile separately. We can thus calculate the dispersion relation at various times during the decompression. Literature values have been used for most parameters, corresponding to the values of temperature and pressure during the decompression (see Fig. 3).

- $\phi = 3 \cdot 10^{-6}$ m^{3}K/J, for a molar volume of 24.9 cm^3/mol.
- $\alpha = 6 \cdot 10^{-5}$ J/m^2, from a direct measurement at 100 mK.[14]

- $D_s = 10^{-11}$ m^2/s, from spin echo measurements on the melting curve at low temperatures.[15]
- $D_l = A(p)/T^2$, with $A(p)$ a pressure dependent constant.[16] During the decompression $A(p)$ varies from 1.7 to 1.9 $\cdot 10^{-11}$ m^{2}K^2/s and D_l from 10^{-7} to 10^{-9} m^2/s.
- $\chi_s = 1/T$; $\chi_l = 5$ K,[16] for $T_F = 200$ mK. In this system of units the Curie constant is 1.
- $V = 15$ μm/s, calculated from both the optical images (Fig. 4) and the magnetization profiles (Fig. 5).
- $\Delta m = 0.6$. The difference in magnetization at the interface at equilibrium is assumed to be constant during the decompression.
- $\frac{\partial m_l}{\partial z}(0)$, the magnetization gradient in the liquid at the interface has been calculated from the magnetization profiles (Fig. 5). It varies from 1700 m^{-1} down to values indistinguishable from zero and has a large margin of error due to the uncertainty of the interface position.

Upon neglecting the small correction of k in the term with the liquid gradient (see equation (18)) we rewrite equation (24) as:

$$\gamma = \frac{V^2}{D_s}\left(\frac{1-\ell_\alpha(k+\frac{V}{2D_l})-\frac{D_l}{D_s(\Delta m)k}\frac{\partial m_l}{\partial z}(0)}{1+\frac{\ell_\alpha V^2}{4D_sD_lk}\left(1+\frac{2\chi_sD_sk}{\chi_lV}\right)}\right) \tag{25}$$

in which the length-scale ℓ_α appears naturally:

$$\ell_\alpha \equiv \frac{\alpha\phi\chi_lD_l}{(\Delta m)^2D_s} \tag{26}$$

Clearly, this is a relevant parameter for the stability of the system: all stabilizing parameters are in the denominator (surface tension, liquid diffusion coefficient); all destabilizing ones are in the numerator (magnetization jump at the interface, solid diffusion coefficient). In equation (25) the term proportional to 1 originates from the solid gradient and the negative ones from the surface tension ($\sim k$) and the liquid gradient ($\sim k^{-1}$). Also, there is a critical velocity $V_c \equiv 2D_l/\ell_\alpha$ above which there can be no instability because the numerator would be negative for each value of k. In this approximation (slowly growing perturbations), above this velocity any perturbations would be surpassed by the macroscopic interface. It has a value of 8 mm/s, which can never be reached experimentally. For reasonable values of the interface velocity we can neglect the term containing V compared to 1 (this implies

$\ell_\alpha \ll 2\ell_l$). It is easy to solve $\gamma(k) = 0$ and we find that γ becomes positive for the first time at $k = 1/2\ell_\alpha$ if:

$$\frac{\partial m_l}{\partial z}(0) = \frac{(\Delta m)^3}{4\alpha\phi\chi_l}\left(\frac{D_s}{D_l}\right)^2 \tag{27}$$

Since the approximate equation (25) is only valid for intermediate values of k and close to the instability, we can not expect reliable outcomes over a wide range. We can however use condition (27) to calculate the time at which the instability should occur. For this, both side of the equation have been plotted against time in Fig. 6, in addition to the values of k at which γ has a maximum (see equation (25)). During the decompression the magnetization gradient in the liquid decreases gradually (see Fig. 5). The increase of the composite parameter is a temperature effect, mainly due to the decrease of D_l. We see that the instability is predicted around 24 s at $k = 5.5 \cdot 10^5$ m^{-1} ($\lambda = 12$ μm). This value satisfies our initial assumption (18), but not convincingly and numerical study is inevitable.

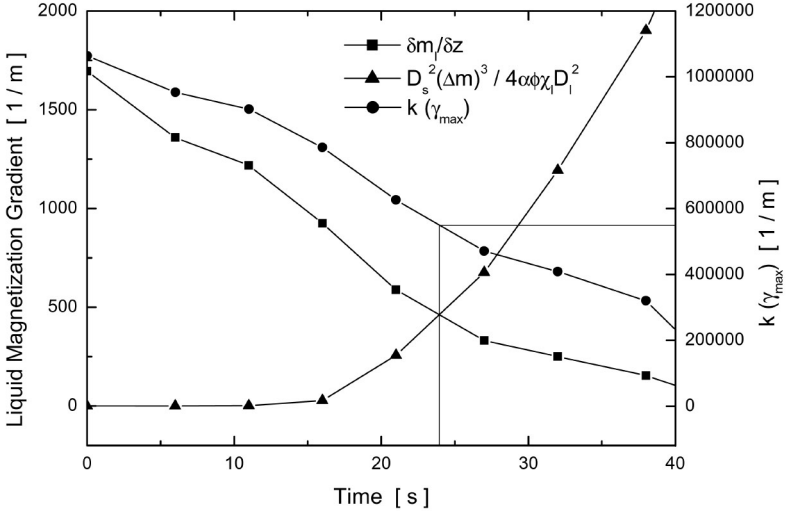

Fig. 6. The decay of the liquid gradient (squares) and the liquid diffusion coefficient, plotted in combination with other parameters (triangles) during decompression. The instability is predicted at the time of intersection of these graphs. The corresponding value of k is estimated from the interpolation of the k-values at maximum γ (circles), obtained graphically from the dispersion relation in the quasi-stationary approximation (25).

4. NUMERICAL ANALYSIS

The set of equations (7), (8) and (16) can be reduced to one implicit equation of degree four in γ by elimination of q_s and q_l. It has been solved numerically at various times during the decompression using the parameter values from the previous section (including the measured liquid gradient at the interface, obtained from Fig. 5). For each point in time γ has been calculated over a wide range of k-values. If the solution is complex, the real part of γ determines whether the perturbation is damped or amplified. From the four sets of solutions $\{q_s, q_l, \gamma\}$ those with $\Re(q_s) > 0$ and $\Re(q_l) > 0$ have been selected. The results are plotted in Fig. 7.

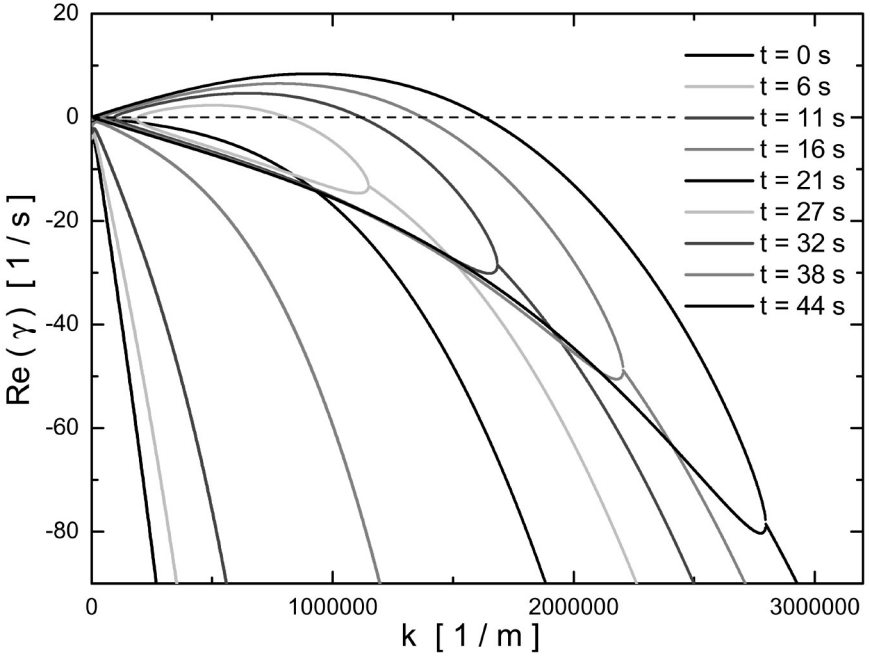

Fig. 7. Graph of the dispersion relation obtained from numerical calculations at various times during decompression. Instability is predicted when the graph crosses the horizontal axis (dotted line), which happens for the first time at $t = 27$ s. At that time the graph has separated into two distinct branches at intermediate values of k.

At the start of the decompression $\Re(\gamma)$ is negative for every value of k. As time progresses the system grows towards instability. After 21 s the

graph splits in two branches. At 27 s the top one has already intersected the horizontal axis and the system has become unstable. By using interpolations we find that $\Re(\gamma)$ is positive for the first time after 25 s for $k = 4.5 \cdot 10^5$ m^{-1}, corresponding to a wavelength of 14 μm. After this the number of unstable modes increases, as does the value of k for which $\Re(\gamma)$ has a maximum.

For very small and very large values of k all three parameters are complex. Complex solutions always form conjugate pairs. As k moves from either side towards the points where the graph splits, the imaginary parts decrease. Between these critical points all parameters values are real. In this region $\Re(\gamma)$ has two different solutions for every value of k, one of which can become positive. Inspection of the solutions shows that the corresponding values of $\Re(q_s)$ are symmetrical in V/D_s. Furthermore, $\Re(q_l) = k$ is a good approximation for each value of k. At very small values of k discontinuities appear.

To investigate the conditions at which instability can occur we varied each parameter while keeping all others constant at various times. Some examples are given in Fig. 8. Increasing D_s increases both the distance between the critical points and the difference between the two solutions. Similarly, increasing α, ϕ, χ_l or D_l has the reverse effect. Variation of V changes the difference between the two solutions, but not the position of the critical points. The system is more sensitive to changes in Δm and less sensitive to those in the liquid gradient. Variations in χ_s have no effect at all. Sometimes there are discontinuities in the lower branch when the corresponding values of $\Re(q_s)$ become negative.

To explain these observations we return to equation (16). Since γ is linear in both q_s and q_l it is obvious that, for a given value of k, all of them are either complex or real. The terms containing the liquid gradient and the surface stiffness are always negative. Because the solid gradient is negative, $\Re(\gamma)$ can only be positive if $\Re(q_s) > V/D_s$. This corresponds with the top branches in Fig. 7. Indeed, at the critical points:

$$q_s = \frac{1}{\ell_s} \tag{28}$$

Then, from equation (5) it follows that $\gamma = -D_s k^2$. These parabolas are sketched in Fig. 8 (dotted lines). They represent an upper limit for the dispersion of a stable system. As we can see from variation of D_s, the critical points are always on these parabolas.

In order to derive an equation for the values of k at the critical points, we substitute $\gamma = -D_s k^2$ and $q_l = k$ in equation (16). All constants and the terms containing χ_s cancel. Again one term is negligible as $\ell_\alpha \ll \ell_l$, and we are left with an equation of degree 3 in k. Since $k = 0$ is not a physical

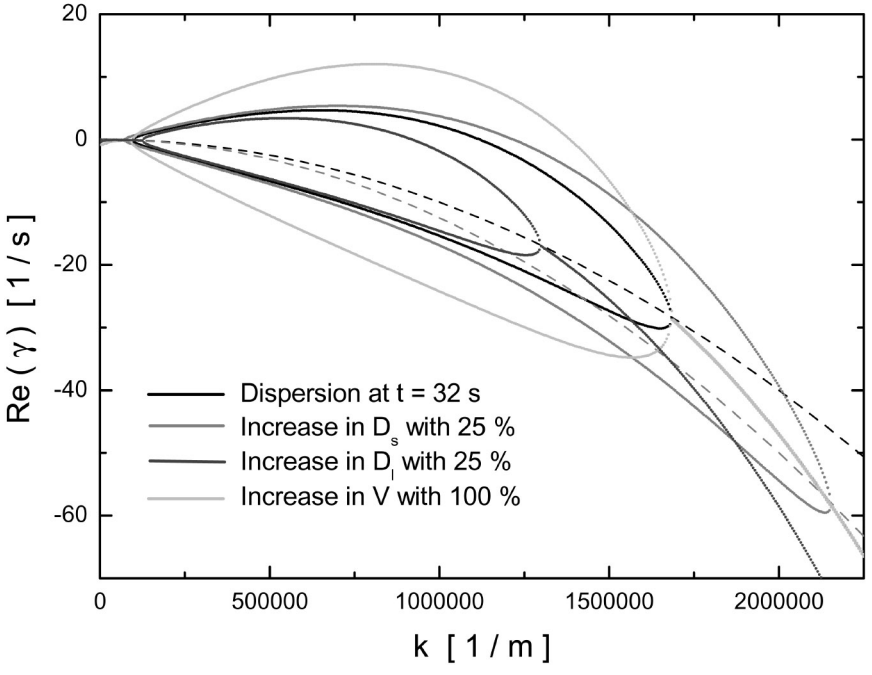

Fig. 8. Variation of three parameters around one solution at a time at which the system is already unstable (black line). An increase in the liquid diffusion stabilizes the system, whereas an increase in the solid diffusion has a destabilizing effect. A change in interface velocity will *not* shift the values of k at which an instability can occur. See text for an explanation of the dotted lines.

solution, we find indeed two k-values:

$$k = \frac{1}{2\ell_\alpha}\left(1 \pm \sqrt{1 - \frac{4\alpha\phi D_l^2 \chi_l}{(\Delta m)^3 D_s^2}\frac{\partial m_l}{\partial z}(0)}\right) \tag{29}$$

This is *exactly* the equation we find when solving $\gamma = 0$ for (25). Note that for our earlier instability condition (27) the square root is exactly zero: for the critical points to exist (correspond with real k-values), the liquid gradient has to be smaller than the combination of parameters plotted in Fig. 6 (the right-hand side of equation (27)). As V and χ_s are not in this expression, a variation in one of these parameters will not change the position of these points. Equation (29) fully determines the topology of the solutions. It enables us to calculate the critical points by hand and understand the

changes in the solutions upon variations, like the strong dependence on Δm and the weak dependence on the liquid gradient. Although the parabola changes slope between the critical points, the point in between is a good indication for the most unstable mode:

$$k(\gamma_{max}) = \frac{1}{2\ell_\alpha} \tag{30}$$

Surprisingly this is the same result as Puech *et al.* found.[7] They also identified the length-scale ℓ_α with the most unstable perturbation, but derived it from different approximations.

5. DISCUSSION

Our theoretical analysis combined with earlier experimental observations[9] has allowed us to verify in amazing detail both the melting scenario proposed by Castaing and Nozières[2] and the instability predicted by Puech *et al.*.[7] By extending their stability analysis to include the transient gradient on the liquid side we have been able to understand the suppression of the Mullins-Serkerka instability[11] during the initial phase of the melting. With literature values for the ^{3}He properties and the measured magnetization gradient in the liquid as input, our calculated dispersion relation is fully consistent with the interpretation of the instability as an interfacial instability driven by the magnetization gradient in the solid.

As far as quantitative agreement is concerned, the calculated value of the most unstable mode (around 15 μm) and the typical scale of the instability (50 - 100 μm) are in the same order of magnitude. This experimental value serves just as an indication; remember that 15 μm is exactly the resolution of our optical system. The time of instability is around 45 s, whereas calculations predict an earlier time (25 s). This might be due to the choice of some of the parameters. As noted before (see equation (29)) the system is quite sensitive to changes in Δm. It is calculated from comparing the bulk magnetization in the solid with that in the liquid at equilibrium (which is 4%) and might be somewhat smaller than 60 %.

More disturbing is the discrepancy between the theoretical and experimental value of the diffusion length in the solid. For our choice of parameters ℓ_s is less than 1 μm. The enhanced magnetization in the surface solid would then be impossible to observe. Even for an entirely flat surface this would be beyond the resolution of the NMR system. However, the boundary layer is clearly visible in Fig. 5, so obviously it is a transient effect. Since we treat each magnetization profile separately, perhaps it would be more justified to estimate the gradient in the solid from our experimental data, as we do for

the liquid. This would then by far be the most uncertain factor, but in any case it would be much smaller than the steady state value. A decrease in the solid gradient would delay the instability even further.

By solving the complete set of equations, we have shown that the quasi-stationary approximation (21) is indeed valid for reasonable choices of the physical parameters. It reproduces the same results in terms of time of instability and most amplified wave-vector. More surprisingly, it produces the *exact* same equation (29) provided we take $q_s = 1/\ell_s$ in the numerical case, instead of the usual $\gamma = 0$. The solid gradient is always negative, since we choose the solid on the right-hand side of the interface. Therefore if $q_s^{-1} > \ell_s$, the first term of the general dispersion relation (16) becomes negative. Evidently, the gradient in the solid can never be *stabilizing* since it is in front of the interface, and we get imaginary solutions. Physically it means that the magnetization decays over a length-scale larger than the diffusion length. In other words, not all of the newly produced magnetization can be transported away through diffusion only, so there is a source. Obviously for a planar solution this is impossible. It is however precisely what we observe in the initial phase of the melting: a build-up of a magnetization layer much thicker than the diffusion length.

The critical case would then correspond to equation (28), where the profile on the solid side would remain unchanged. This is analogous to the situation of so-called "unit undercooling" in case of temperature fields, when the amount of latent heat transported away by diffusion through an undercooled liquid is the same as the amount of heat required to produce solid at its melting temperature. In Fig. 5 we see that after about 20 s the enhanced magnetization starts to decrease from its maximum value of about 2 %, indicating that the system is now in the quasi-stationary regime. After this, provided the gradient in the liquid has decreased sufficiently, the system quickly becomes unstable. The growth will then be determined by the interface kinetics, which is not included in this model.

Finally we would like to remark that dendritic *growth* of ^{3}He was investigated by Rolley *et al.*[12] at $T = 100$ mK. In this situation the sign of both the latent heat and the temperature gradient (solidification gives cooling) are reversed compared to the usual situation, but the experimental results did not differ significantly. However, they noticed a surprisingly weak side branching, probably related to the very weak anisotropy of the surface tension. This is consistent with our observation that the liquid seems to penetrate mostly as cellular dendrites in the solid, with no obvious side branching.

6. ACKNOWLEDGMENTS

We would like to thank A. Marchenkov for contributions in early stages and H. Godfrin and P. Leiderer for useful suggestions. This work was partly supported by the Stichting Fundamenteel Onderzoek van de Materie (FOM), which is financially supported by the Nederlandse Organisatie voor Wetenschappelijk Onderzoek (NWO).

REFERENCES

[§] Present address: Hasbrouck Laboratory, Department of Physics, University of Massachusetts, Amherst, MA 01003, USA.

1. A review is given by G. Bonfait, L. Puech and A. Schuhl, in *Helium Three*, edited by W. P. Halperin and L. P. Pitaevskii (Elsevier Science Publishing, 1990). See also, O. Buu, A.C. Forbes and P.E. Wolf, *Phys. Rev. Lett.* **83**, 3466 (1999); S.A.J. Wiegers, P.E. Wolf and L. Puech, *Phys. Rev. Lett.* **66**, 2895 (1991).
2. B. Castaing and P. Nozières, *J. de Physique* **40**, 257 (1979).
3. G. Vermeulen, S.A. J. Wiegers, C.C. Kranenburg, R. Jochemsen and G. Frossati, *Can. J. Phys.* **65**, 1560 (1987); C.C. Kranenburg, L.P. Roobol, R. Jochemsen and G. Frossati, *J. Low Temp. Phys.* **77**, 371 (1989); O. Buu, L. Puech and P.E. Wolf, *Phys. Rev. Lett.* **85**, 1278 (2000) and references therein.
4. W. van Saarloos, *Phys. Rep.* **301**, 9 (1998).
5. See, e.g., J. S. Langer, *Rev. Mod. Phys.* **52**, 1 (1980); K. Kassner, *Pattern Formation in Diffusion-Limited Crystal Growth* (World Scientific, Singapore, 1996).
6. G. Bonfait, L. Puech, A. S. Greenberg, G. Esaka, B. Castaing, and D. Thoulouze, *Phys. Rev. Lett.* **53**, 1092 (1984).
7. L. Puech, G. Bonfait and B. Castaing, *J. de Physique* **47**, 723 (1986).
8. A. Marchenkov, H. Akimoto, R. van Rooijen, R. Jochemsen and G. Frossati, *Phys. Rev. Lett.* **83**, 4598 (1999).
9. H. Akimoto, R. van Rooijen, R. Jochemsen, G. Frossati and W. van Saarloos, *Phys. Rev. Lett.* **85**, 1894 (2000); H. Akimoto, R. van Rooijen, R. Jochemsen, G. Frossati and W. van Saarloos, in preparation for publication.
10. R. van Rooijen, A. Marchenkov, H. Akimoto, P. Vorselman, R. Jochemsen, G. Frossati, *Physica B* **280**, 561 (2000); R. van Rooijen, A. Marchenkov, H. Akimoto, R. Jochemsen, G. Frossati, accepted for publication in J. Low Temp. Phys..
11. W.W. Mullins and R.F. Sekerka, *J. Appl. Phys.* **35**, 444 (1964).
12. E. Rolley, S. Balibar and F. Graner, *Phys. Rev. E* **49**, 1500 (1994).
13. A. S. Greenberg and G. Armstrong, *Phys. Rev. B* **20**, 1050 (1979).
14. E. Rolley, S. Balibar, F. Gallet, F. Graner, C. Guthmann, *Europhys. Lett.* **8**, 523 (1989).
15. G. Deville, M. Bernier and J.M. Delrieu, *Phys. Rev. B* **19**, 5666 (1979).
16. J. Wilks, *The Properties of Liquid and Solid Helium*, Clarendon Press (1967).